Journal of Instrumentation

Assessment of the effects of different sample perfusion procedures on phase-contrast tomographic images of mouse spinal cord

Published by IOP Publishing for Sissa Medialab

Received: *December 15, 2017*
Accepted: *January 31, 2018*
Published: *March 15, 2018*

International workshop on Imaging II
4–8 September 2017
Varenna, Italy

2018 JINST 13 C03027

Assessment of the effects of different sample perfusion procedures on phase-contrast tomographic images of mouse spinal cord

E. Stefanutti,[a] A. Sierra,[b] P. Miocchi,[a] L. Massimi,[c] F. Brun,[c] L. Maugeri,[a] I. Bukreeva,[c] A. Nurmi,[d] G. Begani Provinciali,[c,e] G. Tromba,[f] O. Gröhn,[b] F. Giove,[g] A. Cedola[c] and M. Fratini[a,c,1]

[a] *IRCCS Fondazione Santa Lucia, Via Ardeatina 306/354, 00142, Roma, Italy*
[b] *Biomedical Imaging Unit, A.I. Virtanen Institute for Molecular Sciences, University of Eastern Finland, Neulaniementie 2, FIN-70211, Kuopio, Finland*
[c] *Institute of Nanotechnology-CNR c/o Physics Department at 'Sapienza' University, Piazzale Aldo Moro 2, 00185 Rome, Italy*
[d] *Charles River Discovery Services, Microkatu 1, 70210 Kuopio, Finland*
[e] *Physics Department at 'Sapienza' University, Piazzale Aldo Moro 2, 00185 Rome, Italy*
[f] *Elettra — Synchrotron Radiation Trieste S.C.p.A, Area Science Park, 34149 Basovizza, Trieste, Italy*
[g] *Centro Fermi-Museo Storico della Fisica e Centro Studi e Ricerche "Enrico Fermi", Piazza del Viminale 1, 00184 Roma, Italy*

E-mail: michela.fratini@gmail.com

Abstract: Synchrotron X-ray Phase Contrast micro-Tomography (SXrPCμT) is a powerful tool in the investigation of biological tissues, including the central nervous system (CNS), and it allows to simultaneously detect the vascular and neuronal network avoiding contrast agents or destructive sample preparations. However, specific sample preparation procedures aimed to optimize the achievable contrast- and signal-to-noise ratio (CNR and SNR, respectively) are required. Here we report and discuss the effects of perfusion with two different fixative agents (ethanol and paraformaldehyde) and with a widely used contrast medium (MICROFIL®) on mouse spinal cord. As a main result, we found that ethanol enhances contrast at the grey/white matter interface and increases the contrast in correspondence of vascular features and fibres, thus providing an adequate spatial resolution to visualise the vascular network at the microscale. On the other hand, ethanol is known to induce tissue dehydration, likely reducing cell dimensions below the spatial resolution

[1]Corresponding author.

https://doi.org/10.1088/1748-0221/13/03/C03027

limit imposed by the experimental technique. Nonetheless, neurons remain well visible using either perfused paraformaldehyde or MICROFIL® compound, as these latter media do not affect tissues with dehydration effects. Paraformaldehyde appears as the best compromise: it is not a contrast agent, like MICROFIL®, but it is less invasive than ethanol and permits to visualise well both cells and blood vessels. However, a quantitative estimation of the relative grey matter volume of each sample has led us to conclude that no significant alterations in the grey matter extension compared to the white matter occur as a consequence of the perfusion procedures tested in this study.

KEYWORDS: Medical-image reconstruction methods and algorithms, computer-aided diagnosis; Medical-image reconstruction methods and algorithms, computer-aided software

2018 JINST 13 C03027

Contents

2018 JINST 13 C03027

1 Introduction

The micro-vascular structural organization of the central nervous system (CNS) plays a significant role both in normal physiological processes [1] and in a broad spectrum of neurovascular and neurodegenerative diseases (e.g. multiple sclerosis, amyotrophic lateral sclerosis, Alzheimer's and Parkinson's diseases) [2], stimulating extensive investigations in this field [3–6]. At the same time, changes in morphological features relative to neuronal network architecture may be indicative of the pathophysiology of many CNS disorders [7]. In particular, in recent years, it has been demonstrated that changes in diffusion magnetic resonance imaging (DTI) parameters [8, 9], as well as in morphological and topological features [10], are the hallmark of axon and myelin integrity and vascular modifications. As a consequence, all these changes clearly correlate with physiopathological alterations occurring in the white (WM) and grey matter (GM). An additional cause often giving rise to important alterations in the morpho-physiology of CNS vascular and neuronal systems is represented by spinal cord injuries (SCIs). SCIs affect both the WM and GM, as well as vascularization, inducing apoptosis of neurons and glial cells, degeneration of WM tracts, WM demyelination, GM dissolution [11–14], and localised disruption of vessels and microvascular networks [15].

As a result, microscale visualization and quantification of the brain and SC vascular and neuronal architecture can provide fundamental information to progress in the comprehension of CNS physiology and to propose new or improved pre-clinical *ex-vivo* investigations of SCI and diseases affecting CNS. Although a number of 2D and non-invasive 3D imaging techniques have been used to define and understand the complex 3D arrangement and morphology of individual neurons, vessels, glia, and axons within the brain and the SC, little progress has been achieved so far, because of the important limitations imposed by conventional approaches. For instance, high-resolution 2D imaging does not yield a complete spatial coverage, likely leading to misinterpretation of the results, while the 3D imaging tools currently available (e.g. MRI, MR angiography, and computed

tomography [16, 17]) do not provide a sufficient spatial resolution and/or an adequate contrast for soft tissues. When higher resolution is achieved by conventional imaging techniques (e.g. scanning electron microscopy, histological sectioning), an invasive or aggressive sample treatment is usually required, such as sectioning, staining, or casting, and only 2D information is derived.

As recently demonstrated, Synchrotron X-ray Phase Contrast micro-Tomography (SXrPCμT) is highly promising for overcoming such limitations [6, 18–21], being it capable to simultaneously visualise the 3D distribution of both the vascular and the neural network in an entire mouse SC with micrometric resolution. This relevant capability of three-dimensional whole sample imaging is particularly suitable for pre-clinical investigations and has already been successfully applied in several applications, such as 3D imaging of liver, tumours, and CNS [21–25]. SXrPCμT does not require sectioning or invasive sample preparation procedures and does not impose the use of contrast agents [19, 21, 26, 27], that often introduce undesired modifications in the sample internal structure and could lead to errors in the qualitative and quantitative interpretation of tomographic images. In addition, SXrPCμT image analysis allows to obtain detailed quantitative information on the neuronal structure, morphology and 3D arrangement (size, density, spatial distribution and correlation) [7], that is expected to be closely related to tissue physiology. The potentiality of such results even exceeds what has been recently obtained by *in-vivo* two-photon microscopy [15], that provides 3D time-resolved information but is restricted by low penetration depth (~100 μm) and limited extension of the region of interest (~ 100–200 μm).

As stated above, one of the key advantages of SXrPCμT without contrast agents is that it represents a non-invasive technique, allowing a direct 3D characterisation of soft tissues at the microscale [10, 21]. However, it is essential to identify optimized experimental strategies in order to improve the achievable contrast-to-noise (CNR) and signal-to-noise (SNR) ratios in order to highlight specific structures. In addition, it needs to be taken into account that SXrPCμT always requires non-invasive sample treatments able to keep all structures stable. This implies that any sample preparation protocol must not involve aggressive procedures inducing possible morphological alterations.

In this framework, the choice of an adequate sample preparation procedure is crucial. Indeed, it has come to light that different sample preparation procedures lead to different features visible in the reconstructed images. Nonetheless, sample preparation methods for SXrPCμT experiments are manifold and can involve a number of variables to take under control, thus an optimized protocol for CNS imaging has not been defined yet.

In this study we report the analysis of the thoracic region of *ex-vivo* mouse SCs, imaged after different sample perfusion procedures. We compare the use of two fixative agents, ethanol and paraformaldehyde (PFA), with MICROFIL® compound (a low-density radio-opaque polymer which enhances the signal coming from vasculature [28]), pointing out that distinct treatments differently affect the WM and GM of SC and result in a different GM/WM contrast. In addition, it emerges that the various agents used in the sample preparation procedure are not capable to make all the different neuronal and vascular network features (vessels, neuronal somas, axons, glial cells) equally visible.

Summarizing, the goals of this paper are: *i)* evaluating the ability of each perfusion procedure to better visualise neuronal cells and vascularization; *ii)* describing the effect of perfusion on the GM morphology and the GM/WM interface, taking advantage of a fast semi-automatic algorithm for the SC GM/WM segmentation and for the quantification of volumes corresponding to WM and GM.

2018 JINST 13 C03027

2 Material and methods

2.1 Sample preparation

Three adult male JAXC57BL/6J (5–6 weeks old, weight 21–28 g, Charles River) mice were used in the study. The animals were housed in a room (22 ± 1°C, 50%–60% humidity) with 12 h light/dark cycle and free access to food and water. All animal procedures were approved by the Animal Care and Use Committee of the Provincial Government of Southern Finland and performed according to the guidelines set by the European Community Council Directives 86/609/EEC.

The mice were anaesthetized intraperitoneally with a ketamine (80 mg/kg)/xylazine (10 mg/kg) mixture and perfused transcardially with 0.9% saline solution containing heparin (50 U/ml) for 3 min at 2 ml/min. After that, the perfusion protocol was as indicated in table 1: the A mouse was perfused with absolute ethanol, the B mouse was perfused with paraformaldehyde, and the last one (mouse C) was perfused with MICROFIL®. The paraformaldehyde (PFA) solution was 4% in 0.1 M phosphate buffer saline (PBS). MICROFIL®, a low-viscosity radio opaque polymer, was purchased from Flow Tech, Inc., Carver, MA. After the perfusion, the SC of each mouse was extracted from the spine and placed in the incubation solution indicated in table 1.

Table 1. List of samples used in our experiments and the preparation protocols. Samples perfused with ethanol, PFA and MICROFIL® are labelled as A, B, and C, respectively.

Mouse	Weight (g)	Procedure	
		Perfusion (2 ml/min)	**Incubation**
A	**27.0**	1) Heparinized saline (3 min) 2) 4% PFA (15 min) 3) Absolute ethanol (10 min)	Absolute ethanol
B	**27.9**	1) Heparinized saline (3 min) 2) 4% PFA (15 min)	4% PFA
C	**21.4**	1) Heparinized saline (3 min) 2) MICROFIL® (15 min)	4% PFA

2.2 Synchrotron X-ray microtomography

In-line synchrotron X-ray phase contrast microtomography (XrPCμT) has been employed to benefit the high image contrast of hard X-rays transparent specimens arising from the sensitivity of a coherent or partially coherent beam to the phase shift induced by the object [22, 29–32]. XrPCμT measurements were carried out at the I13-2 beamline of Diamond Light Source (Harwell Science and Innovation Campus, Oxfordshire, U.K.) and at the SYRMEP beamline of Elettra Light Source (Basovizza, Trieste, Italy). At I13-2 tomographic images were collected using a pseudo-monochromatic X-ray beam with main peak at 14.7 keV and a system of magnification optics connected to a PCO.Edge 5.5 camera to get an affective pixel size of about 1.625 μm; the sample was located 70 cm far from the detector. At SYRMEP a monochromatic X-ray beam at the energy of 25 keV was used, in combination with a sample-detector distance of 1.0 m and a detector pixel size of 4.5 μm. Samples were embedded in agar-agar and included in polypropylene containers; the number of the

2018 JINST 13 C03027

collected projections for each tomography was 2000 at I13-2 and 1440 at SYRMEP. Phase retrieval was performed applying the single distance method proposed by Paganin [33] and all projections were processed and reconstructed using SYRMEP Tomo Project (STP) [34]. We thus obtained a set of high-spatial resolution tomographic images, where the different grey-levels are proportional to the electron density of the different tissues inside the sample. The reconstructed images were analysed by means of ImageJ, using available and home-developed plugins, together with MATLAB® scripts.

2.3 Image segmentation

In order to estimate the WM and GM extension, we developed a software tool for the segmentation of GM and WM [35]. We used this tool to compute the volume occupied by GM and WM in each SC sample. We segmented images obtained by averaging the intensity of a small volume corresponding to a sample thickness of about 85 μm, in the same thoracic region of SC. The tool adopts a procedure corresponding to a "region growing" segmentation method [36, 37] in which a two intensity thresholds are imposed [38]. These thresholds, say t_1 and t_2, are taken as the minimum and the maximum grey levels, respectively, that are found within a rectangular region that is initially selected by the user well inside the area to be segmented. In some cases, when this region is particularly non-uniform, exhibiting grey level peaks, the thresholds are taken as $t_{1,2} = \langle g \rangle \pm 2\sigma$, with $\langle g \rangle$ the average and σ the standard deviation of the grey levels in the region. The "seed" starting point of the algorithm is the upper-right corner of the initially selected region. The adopted region growing method is based on the flooding algorithm (also known as "flood-fill" method, see [39]): starting from the seed point, all the pixels whose grey level lies in the range $[t_1, t_2]$ are considered as belonging to the segmented region, and the pixel selection goes on in a recursive way by selecting only pixels that are the neighbours of those selected in the previous iteration. Hence, the segmented region grows up as a "flood", by enclosing a connected and larger and larger surface, until no more pixels can be selected according to the criterion explained above. Possibly, a "barrier" can be manually selected by surrounding the area of interest with a contour so to avoid that the flooding "overruns" into the background because of the presence of even a few pixels of similar intensity (see the yellow contour in the example of figure 1). At the end, a quantitative measurement is yielded by counting the pixels embedded in the segmented area and the result is converted to a volumetric estimation by multiplying for the sample thickness. We have employed this algorithm to segment both the GM and WM. In order to provide a quantitative (statistical) assessment of the modifications of the distribution of GM with respect to WM, we considered the ratio between the voxel volume assigned to GM and the total volume occupied by SC, given by the sum of GM and WM. An example of GM segmentation is reported in figure 1.

3 Results

We employed XrPCμT for making feasible imaging of *ex-vivo* mouse SCs obtained by perfusion of the samples with ethanol (Mouse A), PFA (Mouse B), and MICROFIL® (Mouse C). We performed our analysis on the whole mouse SC, but we report here only results obtained on a selected region (the thoracic region, by way of example). Such an approach ensured a fair comparison between the different sample preparation procedures employing fixative agents, avoiding misleading

2018 JINST 13 C03027

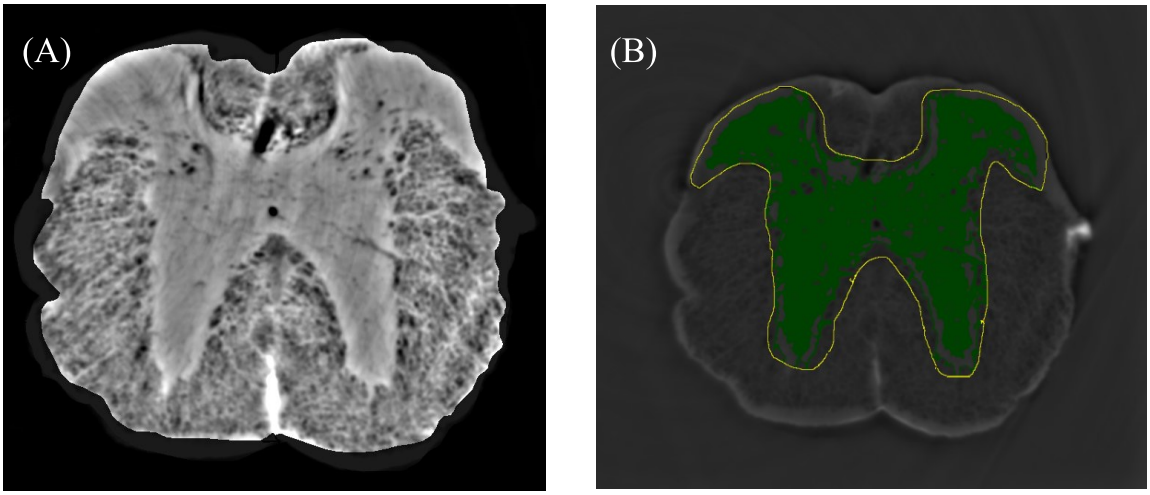

Figure 1. Example of the "flooding" algorithm applied to the GM segmentation of the axial section of a SC imaged at Diamond Light Source. Image (A) displays the average intensity calculated over a stack of consecutive slices corresponding to a volume thickness of about 85 μm. In (B) an example of the application of the home-made ImageJ plugin to the segmentation of GM of the sample in (A) is shown. The yellow solid line was generated by-hand so to avoid that the flooding "overruns" into the background because of the presence of a few pixels of similar intensity connecting the latter with the segmented region.

conclusions due to normal anatomical GM/WM variations occurring across different regions of the SC longitudinal extension.

In order to discuss the different features detectable in the tomographic slices and the variations in GM/WM distribution, we report for each sample the minimum and maximum intensity projections across a reconstructed axial section in the thoracic region of the SC (figures 2–4). A general inspection reveals that all images show a good contrast between WM and GM, even though some differences emerge as a function of the sample preparation procedure adopted. The GM/WM interface appears to be markedly emphasised in the SC perfused with ethanol (figure 2 A–C and F–I), where the H-shaped GM can be clearly distinguished. It further emerges that ethanol perfusion induces a strong increase in tissue rigidity, avoiding vessel walls collapse. As a result, images show the morphology of vasculature features with high contrast, making ethanol perfusion particularly suitable for highlighting the SC vascularization (figure 2 A–E), that distinctly emerges with its vessel and micro-vessel networks providing the blood supply to SC without using contrast agent. On the contrary, ethanol perfusion heavily alters the actual dimensions and 3D morphology of cells, appearing as not appropriate for detecting neurons which are expected to be found in the ventral horn and in the central region of the SC (figure 2F). This is likely due to heavy dehydration experienced by tissues and neuron soma, being water the main constituent of cytosol. As a consequence, neurons become smaller and cannot be resolved because their dimensions are below or close to the spatial resolution limit. Therefore, the absence or marked reduction of water within the neuron somas presumably levels the density differences between the dry soma and the surrounding tissues; this considerably reduces the contrast preventing neurons from being properly imaged. It can be further observed that perfused ethanol also causes a stiffening effect on tissues, especially affecting vessel walls and nerve fibres. However, it is still possible to identify at the GM/WM interface the axonal processes emerging from motor

2018 JINST 13 C03027

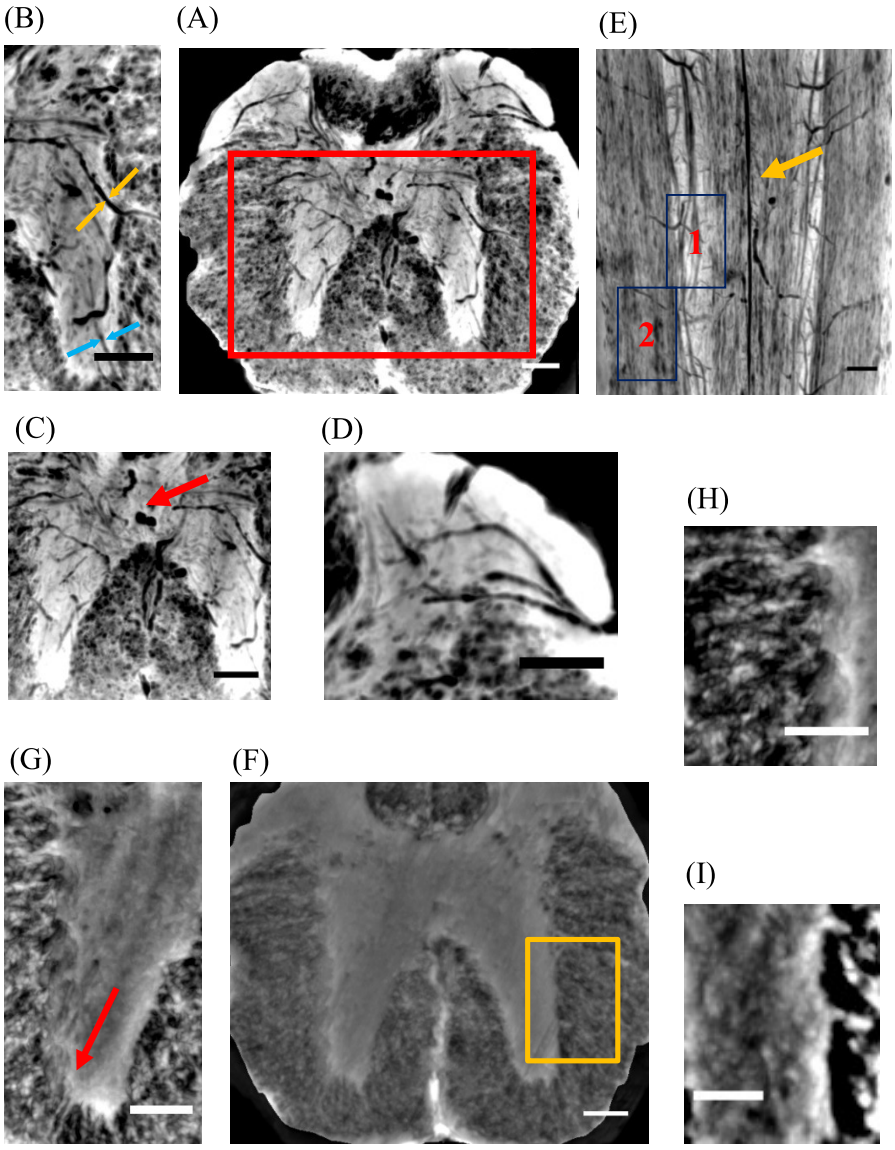

Figure 2. Reconstruction of ~ 400 μm thick volume of the thoracic region of a mouse SC perfused with ethanol (Mouse A), with spatial resolution of 1.625 μm. (A) Axial section of the reconstructed minimum intensity. (B) Enlargement of the right side of the H-shaped GM region, showing in detail the intricate vascularization of SC. Diameter of vessels indicated by yellow and blue arrows is around 11 μm and 5 μm, respectively. (C) Detail of the central region of SC shown in (A), where the transversal section of the central canal is clearly imaged (red arrow). (D) Magnification of the right dorsal horn visible in (A). (E) Longitudinal section of the region selected in (A) (red box): the yellow arrow indicates the central canal, while 1 and 2 mark GM and WM, respectively. In the region corresponding to GM vessels entering/leaving the spinal cord transversally are clearly identified, while in the region corresponding to WM some vertical features are detected, likely representing the axon-bundles (strongly stiffened and heavily dehydrated) running parallel to the longitudinal extension of SC. (F) Axial section of the reconstructed maximum intensity. (G) Enlargement of the left side of (F), focusing on the GM/WM interface. The red arrow points out nerve fibres radially distributed. (H) Detail of the region imaged in (G). (I) Magnification of the region selected in (F) (yellow box), likely depicting two of the axonal processes emerging from motor neurons (not visible) and moving outside the SC, towards the ventral and dorsal root filaments. Scale bars in (A)–(H): 100 μm; scale bar in (I): 50 μm.

2018 JINST 13 C03027

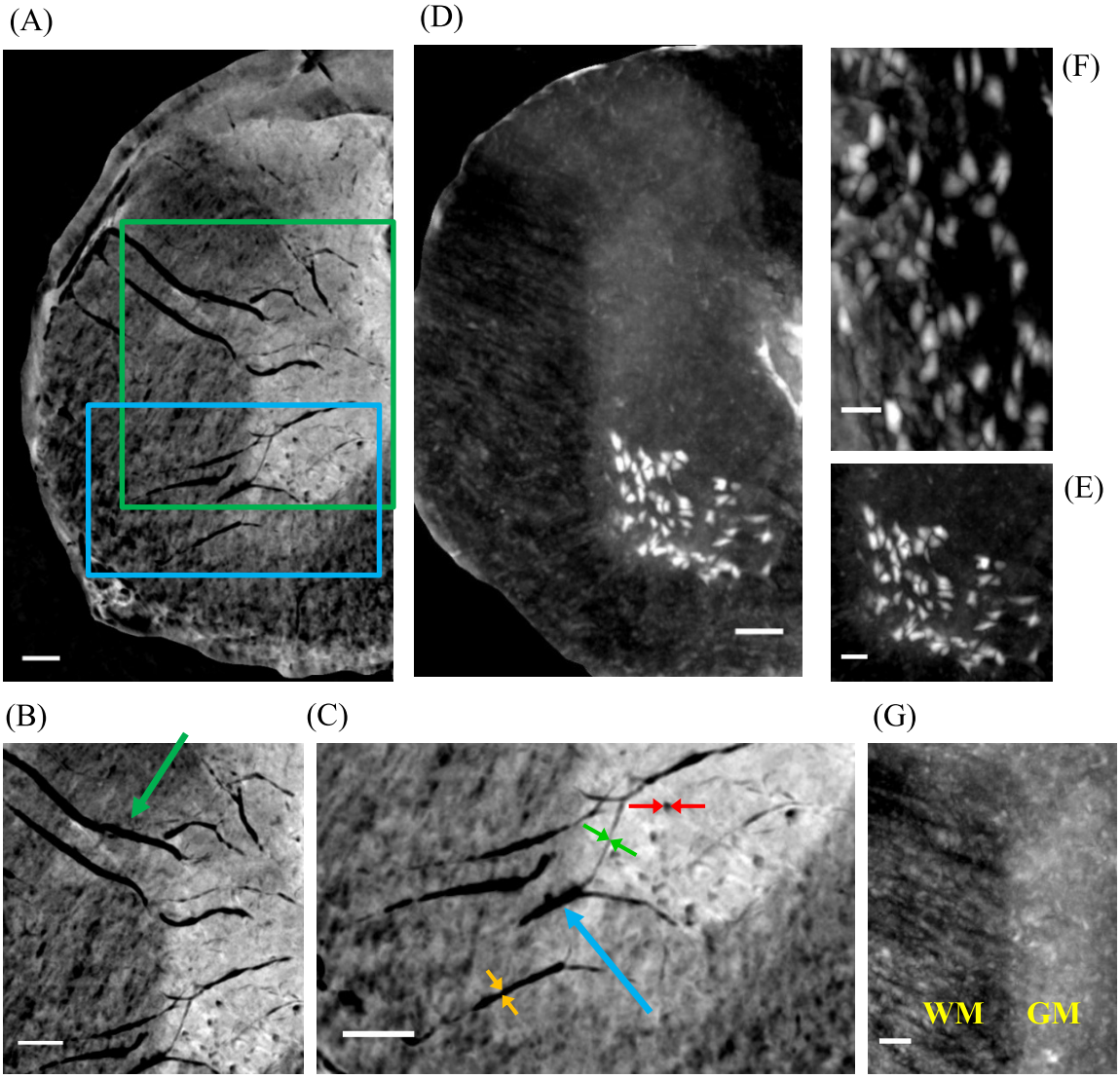

Figure 3. Reconstruction of ~ 400 μm thick volume of the thoracic region of a mouse SC perfused with PFA (Mouse B), with spatial resolution of 1.625 μm. (A) Axial section of the reconstructed minimum intensity. (B), (C) Details imaged in (A) (green and blue boxes) clearly showing the vascular vessel arrangement around the ventral horn and the central region. The GM/WM interface is also visible. The green arrow in (B) points at vessels that are compatible with ramifications of posterior spinal arteries, whereas blue arrows in (C) indicates vessels which might be identified as ramifications of the anterior spinal artery forming the vascular tree penetrating the GM. Red arrows in (C) point at the section of a vessel of ~11 μm in diameter; diameter of vessels indicated by yellow and red arrows is around 10 μm and 5 μm, respectively. (D) Axial section of the reconstructed maximum intensity. (E) Detail of the ventral horn shown in (D) focusing on features compatible with motor neurons (white spots). (F) Longitudinal section of the same volume reported in (E). (G) Enlargement of (D) showing the GM/WM interface. In the region corresponding to WM, glia and nerve fibres radially distributed are visible. Scale bar in (A)–(D): 100 μm; scale bars in (E)–(G): 50 μm.

2018 JINST 13 C03027

neurons (not visible) and moving outside the SC, towards the ventral and dorsal root filaments. Some hints can be captured also by observing the effect on the relative GM spatial distribution: ethanol perfusion produces a manifest shrinking of the GM and WM morphology, to an extent that might be justified with the strong dehydrating effect of ethanol on soft tissues. This behaviour can be visually assessed by comparing figure 2A and figure 2F with any other image here presented. Similarly to what observed with SC perfused with ethanol, PFA perfusion induces a good contrast between GM and WM (figure 3) and enables a clear detection of blood vessels (figure 3 A–C), even though the performance is less amazing than that produced by ethanol. Conversely, PFA perfusion allows not only to visualize the vascular system but also neuronal cells (figure 3 D–F), appearing as white spots much brighter than the surrounding tissues. In particular, knowing that the ventral horn is populated by groups of cells forming the median motor nuclei located in the lamina IX [40], figure 3 E–F clearly point out the presence of cells whose shape, position and dimensions are compatible with motor neurons, whose average size is of the order of 30–50 μm. Likewise, the reconstructed volume of the sample shown in figure 4 shows that MICROFIL® allows to detect motor neurons in the ventral horn. Moreover, as expected, the presence of MICROFIL® enhances the signal due to the microvascular network, making the characteristic "tree" clearly visible both in the maximum and in the minimum intensity projections and highlighting the bifurcation of the central vascularization (figure 4). However, the fine details of the vascular network are missing (figure 4 A–B), as stands out by comparison with results obtained on samples perfused with ethanol and PFA (see figure 2 A–E and figure 3 A–B).

Lastly, in order to quantitatively assess how the sample preparation procedure affects the GM/WM interface, namely the relative extension and distribution of GM with respect to WM, a dedicated ImageJ plugin was developed, allowing the segmentation of GM and the surrounding WM, as described in section2.3. This segmentation algorithm was applied on four sets of slices in the same thoracic region of SC for each sample and the results are depicted in figure 5, where the error bars were defined as the maximum error of the GM volume/SC total volume ratio obtained for each sample.

However, regardless of the results presented in this work, it is needed to be emphasized that the segmentation method here proposed is fast and efficient and can find application also for segmentation of cerebrospinal fluid, WM, and GM in brain images, along with other algorithms proposed in the literature [41–43].

4 Discussion

Recently it has been shown that a fixation procedure can further improve the resolution of XrPCμT images of mice SC tracts and sciatic nerve. In particular, protein and lipid fixation by means of an optimized protocol leads to a better X-ray contrast and a better membrane preservation [44]. On the other hand, the interaction of SC tissues with different agents (even though not contrast agents) is expected to induce alterations in the sample morphology or to differently affect the feasibility of visualizing different features in the neuronal and vascular networks. As a result, a correct comprehension of the effects of sample preparation is crucial to: *i)* correctly evaluate the influence of sample preparation procedures using fixative agents on GM and WM distribution, *ii)* establish sample preparation procedures optimized for the aims of specific experiments. Systematic and exhaustive studies of this issue are still lacking, thus this work is to be intended as one of the first steps in this direction.

2018 JINST 13 C03027

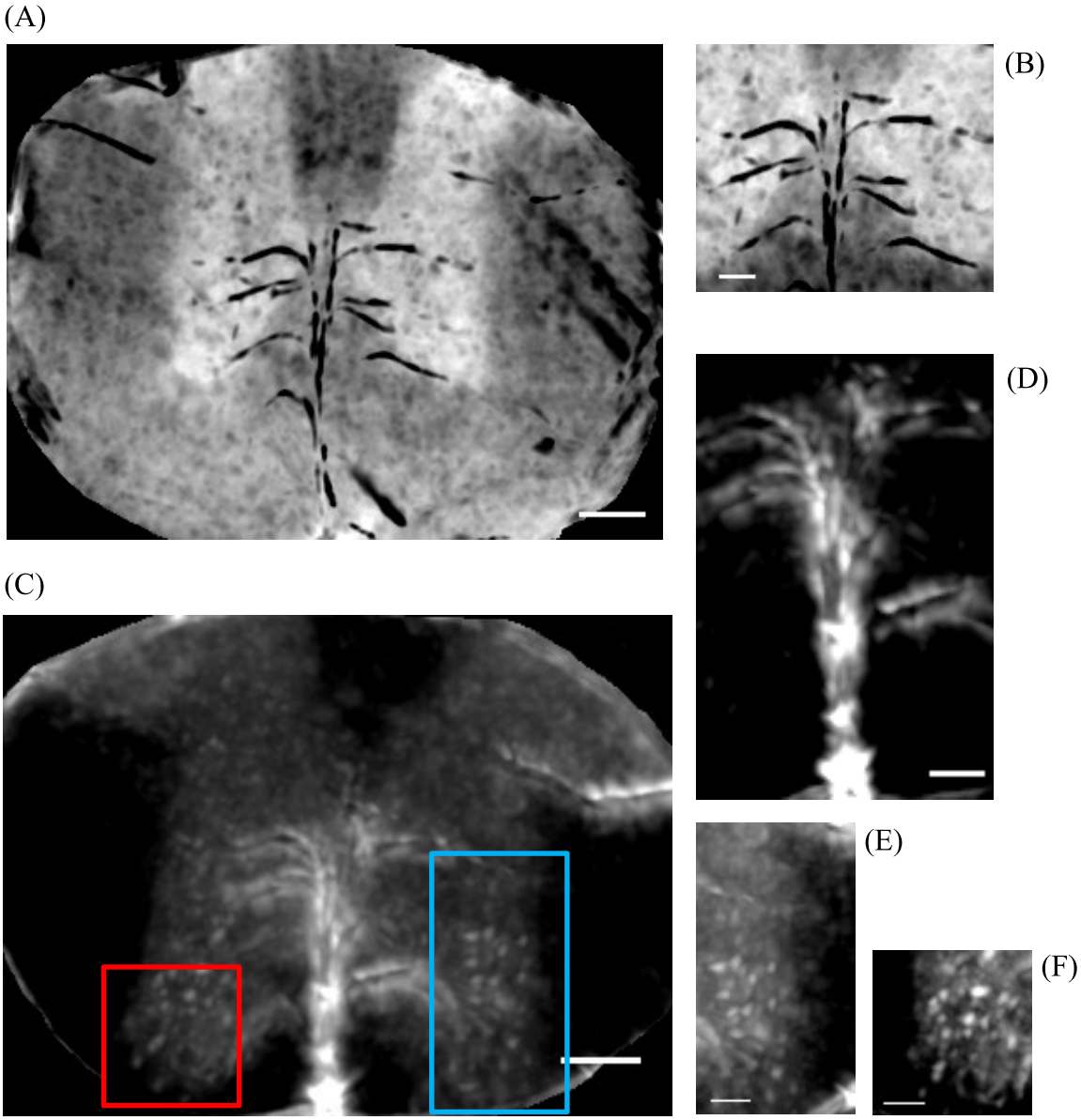

Figure 4. Reconstruction of ~ 1 mm thick volume of the thoracic region of a mouse SC perfused with MICROFIL® (Mouse C), with spatial resolution of 4.5 μm. (A) Axial section of the reconstructed minimum (A) and maximum (C) intensity. The presence of MICROFIL® filling the main vessels evidences the arborescent structure of the vascular tree penetrating the GM. Enlargements of the tree, with the detail of radial vessels, are reported in (B) and (D), where the visible vessels are around 5 μm in diameter. (E), (F) represent the two areas selected in (C): the GM/WM interface is shown, where features compatible with motor neurons (white spots) in the ventral horn can be easily detected. Scale bar in (A) and (C): 100 μm; scale bars in (B) and (D)–(F): 50 μm.

2018 JINST 13 C03027

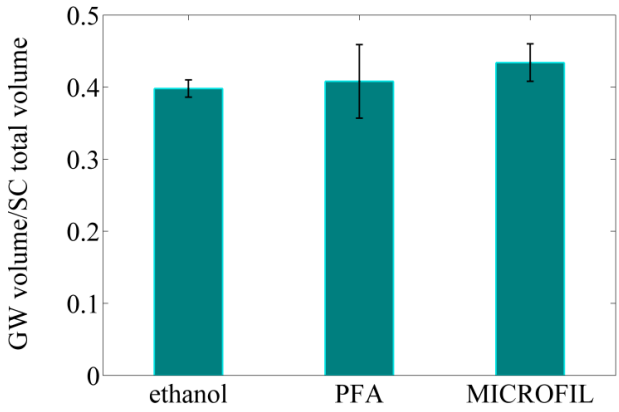

Figure 5. Relative GM volume (calculated with respect to the SC total volume, defined as GM volume + WM volume) evaluated using the home-made ImageJ plugin for the different perfusion protocols described in table 1.

Ex-vivo XrPCμT measurements have made feasible to obtain a 3D reconstruction of several SC samples. In particular, vascular network, nerve fibres, axon-bundles, and neuron soma have been imaged and have resulted to be easily distinguishable at the GM/WM interface. In addition, we found that some perfusion procedures better increase the CNR and are more suitable for visualising neurons, while others reveal better performance in reproducing the vascularization image, as discussed in more detail below.

Investigation of specimens with different sample preparation procedures allowed us to test the effect on SC tissues of MICROFIL® and two fixative agents (ethanol and PFA), evidencing how they differently affect the sample morphology and assessing the ability of the XrPCμT technique in bringing out the diverse morphological features at the microscale. Generally speaking, perfusion seems to be well suitable for visualising the vascular network without contrast agents, in the case of both ethanol and PFA, even though ethanol provides a better result (figure 2 A–E and figure 3 A–C). Interestingly, sample preparation obtained using ethanol under perfusion exhibits a marked increase in the tissue rigidity, including the vessel walls. This effect efficiently circumvents the problem of vessel collapse, increases the SNR and allows to properly visualize the vascular network avoiding the use of contrast agents. Moreover, perfused ethanol produces a strong contrast between GM and WM, but at the same time it seems to induce a simultaneous shrinking of the GM and WM volume (figure 2). Perfusion with ethanol shows a further limitation: cells cannot be distinctly resolved, probably because of dehydration that lowers the obtainable CNR and reduces neuron dimensions below the resolution limit (figure 2 F–I). Perfusion with PFA can make up for this important shortcoming: figure 3 E–F distinctly indicates the presence of motor neurons in the ventral horn, while figure 3 A–C allows for visualizing in detail the vascularization (even though less evident with respect to ethanol), with a good contrast between GM and WM. The neuronal population can also be retrieved by injecting MICROFIL® compound, as shown in figure 4 C–F. With reference to vascularization detection, figure 4 A–B shows how MICROFIL® enhances the contrast of blood vessels. However, it is worth observing that the sample preparation involving perfusion with MICROFIL® is not trivial and less reliable with respect to the fixative agents used in this study. If MICROFIL® is

2018 JINST 13 C03027

allowed to well penetrate vessels at all scales up to small capillaries, the resulting tomographic image might be of superlative quality and profuse in useful and detailed information, as reported in previous experiments [21]. Nonetheless, the probability to obtain a MICROFIL® perfused SC of high quality is quite low because very often MICROFIL® fails in filling the vessels, especially the smallest ones, or spills out from cracks or discontinuities in vessel walls of damaged or injured samples.

Since by visual inspection the different procedures adopted for sample preparation seem to especially affect the morphology and the volume extent of GM, we quantified for each sample the GM relative volume (defined as GM volume/SC total volume, where SC total volume is given by the sum of GM and WM volumes) evaluated on a series of axial sections ($\sim 85\,\mu$m thick) in the thoracic region of the SC. We performed this assessment using our ImageJ plugin described in section 2.3. In fact, all our specimens were derived from three mice with the same characteristics (species, sex, age, weight), which underwent the same treatment before perfusion. This implies that it is reasonable to expect that the proportion of GM/(GM+WM) *before* perfusion is the same within the experimental errors, also accounting for the unavoidable biological variability. As a result, if any significant difference in the GM/(GM+WM) ratio is observed across our specimens, it would be explained as due to the specific perfusion protocol. However, despite we have previously observed that ethanol perfusion induces morphological modifications in GM and stiffening effects on tissues due to dehydration, a quantitative analysis reveals that shrinking simultaneously affects both the GM and WM. In fact, our segmentation algorithm has evidenced no significant differences between the relative GM volume extent across different sample preparation procedures, as shown in figure 5, where the GM relative volumes calculated for the three sample treatments are the same within the experimental errors.

Nonetheless, it should be noted that this outcome might descend from high relative errors associated with each measure. However, this is not due to an intrinsic variability in the pixel intensity from the reconstructed slices of the samples, but rather to the different contrast between GM and WM revealed by each sample preparation procedure. In particular, perfusion with ethanol is able to greatly enhance the GM/WM contrast, reducing the uncertainty of the flooding algorithm in identifying pixels corresponding to GM or WM. Conversely, sample perfused with PFA reveals a less pronounced GM/WM contrast, as well as the sample perfused with MICROFIL®, whose GM/WM contrast is further worsened by image artifacts and lower resolution affecting tomographic images collected at Elettra. This clearly led to a higher uncertainty in the segmentation procedure and in the calculation of the corresponding GM and WM volume, that could, in turn, make differences not appreciable.

5 Conclusions

In this work we show tomographic images of the thoracic region of *ex-vivo* mouse SCs obtained by means of the synchrotron-based phase-contrast tomography, which allows to investigate simultaneously vascular and neuronal networks avoiding contrast agents and invasive sample treatment procedures. Therefore, we performed a series of three non-invasive sample treatments testing how they lead to images capable to highlight different features and showing that the choice of a fixative agent over another can make a difference in what a given experiment may tell us. In particular, we assessed the effect of sample perfusion with two different fixative agents (ethanol and PFA) and MICROFIL® on the feasibility of detecting the vasculature, the neuronal network, and the GM/WM interface.

2018 JINST 13 C03027

We have pointed out that perfusion with ethanol induces a strong increase in tissue rigidity, avoiding vessel collapse. This result demonstrates that perfusion with ethanol represents a well-suited strategy for imaging vasculature without using contrast agents. Thus, if the target of the experiment is to visualize the vascular network or enhance the GM/WM interface, perfusion with ethanol might be the best choice, giving access to the actual morphology of the vascular features thanks to the higher tissues rigidity preventing vessel walls collapse. Perfusion with PFA appears as the halfway solution: it simultaneously provides information about vascularization and permits to detect motor neurons, preserving a sensible GM/WM contrast. For neuronal cells and vascularisation, perfusion with PFA is likely to be preferred even to perfusion with MICROFIL®, as the latter often entails the uncertainties and experimental difficulties discussed in the previous section. Moreover, PFA is to be regarded as the most versatile fixative agent as it can be also employed in other experimental techniques, such as MRI, allowing for multimodal approaches. Combining all results, it clearly emerges that the sample should be prepared on the basis of the specific aims of the experiment.

Finally, we attempted to quantify changes induced by ethanol, PFA, and MICROFIL® on the relative GM volume using a segmentation algorithm for properly detecting the GM/WM interface. Despite a visual inspection seems to demonstrate that perfused ethanol is responsible for morphological modification of GM resulting in a shrinking effect, no dramatic differences in the GM/WM volume ratio among the different sample preparation procedures here investigated have been revealed. We can thus conclude that the three different perfusion protocols here tested affect the percentage of WM and GM of mouse spinal cord in the same manner, within the experimental errors.

This report intends to be a guide for establishing the best sample preparation protocol as a function of the features one is interested to observe, taking under consideration that any experiment requires some compromises. The idea is thus to allow for designing more efficiently targeted XrPCμT experiments in the next future. We also give a reference for evaluating which changes a specific perfused agent (ethanol, PFA, MICROFIL®) is expected to produce on vascular and cellular features and on the GM/WM interface.

Our results might provide relevant information for assessing new and improved therapeutic strategies and for better understanding pathological mechanisms and their evolution.

Acknowledgments

Authors wish to thank the I13-2 and SYRMEP beamlines, at the Diamond Light Source and Elettra Light Source, respectively, for providing beamtime. They are also grateful to both the beamline staffs for their helpful scientific and technical support. In addition, they would like to thank Maarit Pulkkinen for her help with the animal handling.

The present work was supported by the Italian Ministry of Health under the Young Researcher Grant 2013 (GR-2013-02358177) to M. F. Part of research reported in this publication was also supported by the the European project VOXEL (HORIZON 2020-Fet Open; Project reference: 665207). Part of this work has received funding from the European Union Horizon 2020 research and innovation programme under the Marie Skłodowska-Curie grant agreement No 691110 (MICROBRADAM). A. Sierra also acknowledges the Academy of Finland (#275453) for financial support.

2018 JINST 13 C03027

References

[1] Y. Ge et al., *Age-related total gray matter and white matter changes in normal adult brain. Part I: volumetric MR imaging analysis*, *Am. J. Neuroradiol.* **23** (2002) 1327.

[2] R. Weissleder and U. Mahmood, *Molecular imaging*, *Radiology* **219** (2001) 316.

[3] B. V. Zlokovic, *The blood-brain barrier in health and chronic neurodegenerative disorders*, *Neuron* **57** (2008) 178.

[4] B. V. Zlokovic, *Neurovascular pathways to neurodegeneration in alzheimer's disease and other disorders*, *Nat. Rev. Neurosci.* **12** (2011) 723.

[5] S. Heinzer, T. Krucker, M. Stampanoni, R. Abela, E. P. Meyer, A. Schuler et al., *Hierarchical microimaging for multiscale analysis of large vascular networks*, *NeuroImage* **32** (2006) 626.

[6] F. Plouraboué, P. Cloetens, C. Fonta, A. Steyer, F. Lauwers and J.-P. Marc-Vergnes, *X-ray high-resolution vascular network imaging*, *J. M.icrosc.* **215** (2004) 139.

[7] I. Bukreeva, G. Campi, M. Fratini, R. Spanò, D. Bucci, G. Battaglia et al., *Quantitative 3d investigation of neuronal network in mouse spinal cord model*, *Sci. Rep.* **7** (2017) 41054.

[8] J.H. Kim, M.D. Budde, H.-F. Liang, R. S. Klein, J.H. Russell, A.H. Cross et al., *Detecting axon damage in spinal cord from a mouse model of multiple sclerosis*, *Neurobio. Dis.* **21** (2006) 626.

[9] J.H. Kim, D.N. Loy, H.-F. Liang, K. Trinkaus, R.E. Schmidt and S.-K. Song, *Noninvasive diffusion tensor imaging of evolving white matter pathology in a mouse model of acute spinal cord injury*, *Magn. Reson. Med.* **58** (2007) 253.

[10] A. Cedola, A. Bravin, I. Bukreeva, M. Fratini, A. Pacureanu, A. Mittone et al., *X-ray phase contrast tomography reveals early vascular alterations and neuronal loss in a multiple sclerosis model*, *Sci. Rep.* **7** (2017) 5890.

[11] N.A. Silva et al., *From basic to clinical: A comprehensive review on spinal cord injury*, *Prog. Neurobiol.* **114** (2014) 25.

[12] E. Park, A. A. Velumian and M. G. Fehlings, *The role of excitotoxicity in secondary mechanisms of spinal cord injury: A review with an emphasis on the implications for white matter degeneration*, *J. Neurotrauma* **21** (2004) 754.

[13] J.W. McDonald and C. Sadowsky, *Spinal-cord injury*, *The Lancet* **359** (2002) 417.

[14] B. Winter, H. Pattani and E. Temple, *Spinal cord injury*, *Anaesth. Intensive Care Med.* **15** (2014) 424.

[15] C. Dray, G. Rougon and F. Debarbieux, *Quantitative analysis by in vivo imaging of the dynamics of vascular and axonal networks in injured mouse spinal cord*, *Proc. Natl. Acad. Sci.* **106** (2009) 9459.

[16] I. Sigel et al., *Essential Neuroscience*, Walters Kluwe, 2004.

[17] F. Kiessling, S. Greschus, M.P. Lichy, M. Bock, C. Fink, S. Vosseler et al., *Volumetric computed tomography (VCT): a new technology for noninvasive, high-resolution monitoring of tumor angiogenesis*, *Nat. Med.* **10** (2004) 1133.

[18] A. Bravin, P. Coan and P. Suortti, *X-ray phase-contrast imaging: from pre-clinical applications towards clinics*, *Phys. Med. Biol.* **58** (2012) R1.

[19] J.-Z. Hu, T.-D. Wu, L. Zeng, H.-Q. Liu, Y. He, G.-H. Du et al., *Visualization of microvasculature by x-ray in-line phase contrast imaging in rat spinal cord*, *Physi. Med. Biol.* **57** (2012) N55.

[20] A. Momose, *Recent advances in x-ray phase imaging*, *Jpn J. App. Phys.* **44** (2005) 6355.

2018 JINST 13 C03027

[21] M. Fratini, I. Bukreeva, G. Campi, F. Brun, G. Tromba, P. Modregger et al., *Erratum: Corrigendum: Simultaneous submicrometric 3d imaging of the micro-vascular network and the neuronal system in a mouse spinal cord*, *Sci. Rep.* **5** (2015) 8514.

[22] A. Momose, T. Takeda, Y. Itai and K. Hirano, *Phase-contrast X-ray computed tomography for observing biological soft tissues*, *Nat. Med.* **2** (1996) 473.

[23] B. Müller et al., *High-resolution tomographic imaging of microvessels*, *Proc. SPIE* **7078** (2008) 70780B.

[24] S. Lang, B. Müller, M. D. Dominietto, P. C. Cattin, I. Zanette, T. Weitkamp et al., *Three-dimensional quantification of capillary networks in healthy and cancerous tissues of two mice*, *Microvasc. Res.* **84** (2012) 314.

[25] P. Carmeliet et al., *Angiogenesis in cancer and other diseases*, *Nature* **407** (2000) 249.

[26] A. Momose, T. Takeda and Y. Itai, *Blood vessels: Depiction at phase-contrast x-ray imaging without contrast agents in the mouse and rat—feasibility study*, *Radiology* **217** (2000) 593.

[27] T. Takeda, *Vessel imaging by interferometric phase-contrast x-ray technique*, *Circulation* **105** (2002) 1708.

[28] S.X. Vasquez, F. Gao, F. Su, V. Grijalva, J. Pope, B. Martin et al., *Optimization of MicroCT imaging and blood vessel diameter quantitation of preclinical specimen vasculature with radiopaque polymer injection medium*, *PLoS ONE* **6** (2011) e19099.

[29] S. Mayo, T. Davis, T. Gureyev, P. Miller, D. Paganin, A. Pogany et al., *X-ray phase-contrast microscopy and microtomography*, *Opt. Express* **11** (2003) 2289.

[30] A. Olivo and E. Castelli, *X-ray phase contrast imaging: from synchrotrons to conventional sources*, *Riv. Nuovo Cim.* **37** (2014) 467.

[31] S.-A. Zhou and A. Brahme, *Development of phase-contrast x-ray imaging techniques and potential medical applications*, *Phys. Med.* **24** (2008) 129.

[32] P. Cloetens, R. Barrett, J. Baruchel, J.-P. Guigay and M. Schlenker, *Phase objects in synchrotron radiation hard x-ray imaging*, *J. Phys.* **D 29** (1996) 133.

[33] D. Paganin, S.C. Mayo, T.E. Gureyev, P.R. Miller and S.W. Wilkins, *Simultaneous phase and amplitude extraction from a single defocused image of a homogeneous object*, *J. Microsc.* **206** (2002) 33.

[34] F. Brun, L. Massimi, M. Fratini, D. Dreossi, F. Billé, A. Accardo et al., *SYRMEP tomo project: a graphical user interface for customizing CT reconstruction workflows*, *Adv. Struct. Chem. Imag.* **3** (2017) 4.

[35] D. Barber, *Fundamentals of medical imaging: Paul Suetens*, *Med. Eng. Phys.* **25** (2003) 161.

[36] T.S. Yoo, *Insight into images: Principles and Practice for Segmentation, Registration, and Image Analysis*, AK Peters/CRC Press (2004).

[37] B. Preim and C. Botha, *Visual Computing for Medicine, Theory, Algorithms, and Applications*, Morgan Kaufmann (2017).

[38] T. Boskamp, D. Rinck, F. Link, B. Kümmerlen, G. Stamm and P. Mildenberger, *New vessel analysis tool for morphometric quantification and visualization of vessels in CT and MR imaging data sets*, *RadioGraphics* **24** (2004) 287.

[39] T. Shane, *Applied Computer Science*, Springer (2016).

2018 JINST 13 C03027

[40] E.R. Kandel et al., *Principles of Neural Sciences*, 4th ed., McGraw-Hill Medica (2000).

[41] K.O. Lim and A. Pfefferbaum, *Segmentation of MR brain images into cerebrospinal fluid spaces, white and gray matter*, *J. Comput. Assist. Tomogr.* **13** (1989) 588.

[42] M.E. Brandt, T.P. Bohant, L.A. Kramer and J.M. Fletcher, *Estimation of CSF, white and gray matter volumes in hydrocephalic children using fuzzy clustering of mr images*, *Comput. Med. Imaging Graph.* **18** (1994) 25.

[43] A. Pfefferbaum, K.O. Lim, R.B. Zipursky, D.H. Mathalon, M.J. Rosenbloom, B. Lane et al., *Brain gray and white matter volume loss accelerates with aging in chronic alcoholics: A quantitative MRI study*, *Alcohol. Clin. Exp. Res.* **16** (1992) 1078.

[44] P. Parlanti, V. Cappello, F. Brun, G. Tromba, R. Rigolio, I. Tonazzini et al., *Size and specimen-dependent strategy for x-ray micro-ct and tem correlative analysis of nervous system samples*, *Sci. Rep.* **7** (2017) 2859.

2018 JINST 13 C03027